Journal of Alloys and Compounds 768 (2018) 349–357

Contents lists available at ScienceDirect

Journal of Alloys and Compounds

journal homepage: http://www.elsevier.com/locate/jalcom

Heterogeneity of strain path, texture and microstructure evolution of AA6063-T6 processed by Equal Channel Angular Sheet Extrusion (ECASE)

Jairo Alberto Muñoz*, Martina Avalos, Raúl E. Bolmaro

Instituto de Física Rosario, Consejo Nacional de Investigaciones Científicas y Técnicas-CONICET, Universidad Nacional de Rosario, Ocampo y Esmeralda, 2000 Rosario, Argentina

ARTICLE INFO

Article history:
Received 18 April 2018
Received in revised form
16 July 2018
Accepted 18 July 2018
Available online 24 July 2018

Keywords:
Aluminum
Strain
Grain size
Texture
Dislocations

ABSTRACT

An Aluminum alloy 6063T6 was processed at room temperature by Equal Channel Angular Sheet Extrusion (ECASE). Microstructure evolution was investigated by Electron Back Scattering Diffraction (EBSD), and X-ray diffraction analysis. The texture evolution was heterogeneous and represented by a mix of rolling and shearing components through the sheet thickness. Ncorr™ calculations showed higher shear strains close to the edges than in the sheet core, in agreement with the through thickness expected variation. The Geometrically Necessary Dislocation (GND) calculations corroborated the existence of a heterogeneous microstructure through the sheet thickness.

1. Introduction

Materials processed by Severe Plastic Deformation (SPD) techniques present interesting behavior not only because of the very low amount of porosity but also for their mechanic properties. However, severe plastic deformation leads to an increase in the strength of the metallic materials but at the same time also reduces the homogeneous deformation zone leading to lower ductility. Another issue related with the production of Ultra Fine Grain (UFG) materials is the mass productivity of high quality material when manufactured by SPD techniques, since the processing demands are highly increased with the dimensions of the processed material.

For solving this problem, some new SPD techniques based on the original principles of shear strain have been proposed. Equal Channel Angular Rolling (ECAR) [1,2] and Equal Channel Angular Drawing of Sheet or Sheet Extrusion (ECADS or ECASE) [3] are some of these Equal Channel Angular Pressing (ECAP) modified techniques. These processes allow the production of larger ultrafine microstructure sheets. In the ECASE process the deformation is a function upon both the shearing (γ) and the extrusion (ε_y) components as equation (1) shows [3]:

$$\varepsilon = \frac{\gamma}{\sqrt{3}}\left[1+4\left(\frac{\varepsilon_y}{\gamma}\right)^2\right]^{1/2} \approx \frac{\gamma}{\sqrt{3}}\left[1+2\left(\frac{\varepsilon_y}{\gamma}\right)^2\right] \quad (1)$$

where $\gamma = 2\tan\left(90^\circ - \phi/2\right)$ and $\phi = 150^\circ$, for the current experiments.

In this way, the effective strain per ECASE pass can be estimated as ~0.31 [3]. Nowadays, different studies are more focused in the initial stages of deformation like one ECAP pass [4] or the use of modified conventional methods, like differential speed rolling [5].

According with Ma et al. [6], in a heterogeneous structure both soft and hard regions can coexist (e.g., small and large grains) with the soft regions plastically deforming more than hard ones giving rise to gradients of plastic deformation. As Ashby [7] established, the accommodation of such plastic gradients requires the storage of geometrically necessary dislocations, which contribute to work hardening, with the characteristic length scale of gradient plastic deformation determined by the spacing between neighboring soft and hard regions. According to Ashby [7], heterogeneous nanostructures are characterized by unusually small length scale of gradient plastic deformation, and thus offer a high capacity of

* Corresponding author.
E-mail addresses: munoz@ifir-conicet.gov.ar (J.A. Muñoz), avalos@ifir-conicet.gov.ar (M. Avalos), bolmaro@ifir-conicet.gov.ar (R.E. Bolmaro).

https://doi.org/10.1016/j.jallcom.2018.07.216
0925-8388/

storing more geometrically necessary dislocations, thereby enhancing the strain hardening and consequently a good combination of strength and ductility.

For the current experiments, it is speculated that such effect, induced in the surfaces of the sheets, would be combined with the properties of the core material with larger sub-grains, capable of absorbing more defects, simultaneously constrained by the surface layers and gradually being incorporated to them while the deformation proceeds, either by further deformation or by forming operations.

Aluminum alloys are used in a variety of structural applications ranging from building and automotive to aerospace industries [8]. Al-Mg-Si alloys are among the most used aluminum alloys due to their attractive combination of mechanical properties, corrosion resistance, extrudability and excellent response to the surface finishing operations.

The aim of this work is the study of the texture and microstructural evolution of the AA6063T6 processed by the ECASE process at room temperature and the strain characterization showing that this process can be a good alternative to produce heterogeneous microstructures. According with some new research [6,9] a heterogeneous microstructure can be a good option to produce materials with good strength and ductility, simultaneously. The current approach explores the possibility of inducing heterogeneity according to two different meanings: heterogeneous grain sizes and heterogeneous spatial distribution of those different grain sizes.

Effectively, one ECASE pass, with 0.31 effective strain, does not represent severe plastic deformation, although the technique is actually designed with that purpose. However, the main goal of this study is not achieving high material deformation, or bulk severely deformed material, but investigating the effectiveness of its first stages to generate heterogeneity in the material. Larger deformations, by increasing the number of passes, should allow to controllably introducing more material from the core of the sheet while still keeping certain pre-designed heterogeneity.

2. Experimental procedure

A 6063T6 Al alloy (0.35%Fe; 0.2–0.6%Si; 0.1%Mn; 0.45–0.9%Mg; 0.1%Cr; 0.1%Zn; 0.1%Ti; 0.1%Cu; Al (in wt %)) was received in the form of sheets with 38 mm width and 3 mm thickness. Before the ECASE process, the material was heat treated at 530 °C for 4 h and further water quenched, followed by heating at 190 °C for 10 h and air cooling. ECASE was carried out at room temperature using two parts die with an inner angle of $\Phi = 150^\circ$ (see Fig. 1a), resulting in a true strain of ~0.31 per pass according to Zisman et al. [3]. This strain value is lower than the values obtained by most of the SPD techniques such as ECAP [10], High Pressure Torsion (HPT) [11] and Accumulative Roll Bonding (ARB) [12]. However, the main goal of the current study is not obtaining high material deformation and ultrafine microstructure through repetitive ECASE passes (i.e. smaller and homogeneous grain size). Alternatively, lower deformations were used to search for processes to generate heterogeneity in the material. Molybdenum disulfate (MoS_2) was used as a lubricant to minimize the friction between the die and the workpiece.

The microstructure of the samples was characterized by Electron Backscattered Diffraction (EBSD). For this purpose, specimens were cut from the TD plane of the ECASE samples (see Fig. 1b) and mechanically polished from 2500 grit SiC paper until 0.02 μm colloidal silica suspension. The data was processed with TSL OIM 7.3b software. The data processing parameters for OIM software were: maximum misorientation threshold angle of 5° for grain size calculation and clean-up subroutine by grain dilation with a minimum grain size of 4 points. For characterizing the local texture five EBSD maps (S1, S2, S3, S4 and S5) were obtained with 1 μm step size covering the full sheet thickness. Misorientations lower than 0.5° were not considered in the data post-processing. The orientation distribution functions (ODFs) were calculated by series expansion method using truncation at $L = 22$ (L represents the truncation error because the series expansion method has to be truncated to a limited number of terms to keep the computation time to practical limits. In practical terms, a value of $Lmax = 22$ is generally taken as a limit for cubic materials) [13,14].

The X-ray diffraction measurements of the processed samples were carried out on a Philips X pert Pro MPD diffractometer with Cu-Kα radiation, X-ray lenses, parallel plate collimator and Xe detector. The array was the one known as Schulz reflection method This method was designed for determining pole figures of flat samples with a Geiger counter x-ray spectrometer. In the modern setup, the main advantage of the method is that the experimental data can be used directly without corrections for changes in geometry during tilting of the sample [15,16]. The specimens were mechanically polished to 1000 grit and then etched with Kellers solution (Fig. 1b). The initial three measured pole figures were corrected for defocusing and further analyzed by WXpopLA [17] and MTEX [18] tool box. Seven samples were analyzed in the rolling plane (⊥ ND plane) at different depths to wit: inner edge surface, 0.4 mm, 0.8 mm, 1.2 mm, 1.6 mm, 2 mm down from the inner surface and the outer edge surface; and one more in the shearing plane (⊥ TD plane).

The strength of the processed material was characterized by hardness measurements in the Knoop scale. Three different hardness profiles were done along the sheet thickness to evaluate the hardening gradient between the zones closer to the edges and the sheet core.

To study the deformation introduced through the ECASE process, the free software Ncorr™ [19] was used (see Fig. 1c). With Ncorr™ software the distribution of the deformation is obtained by Digital Image Correlation (DIC) [20] applied to a random pattern of black spots over a white color surface in the TD plane before and after the deformation process was carried out. During the deformation, test pictures were taken every two seconds. In that way, the deformation is obtained by the comparison of the change in the black spots shape and position in an area before and after deformation (see Fig. 1d).

3. Results and discussion

3.1. Strain during ECASE process

Fig. 2 shows the strain distribution calculated by Ncorr™ for the first ECASE pass. The results obtained with this analysis indicate that the shear strain values are higher in the edges than in the center of the sheet, proving that the ECASE process can introduce more deformation in the material surfaces than in its core due to the shearing effect because of the ECASE die. These results also confirmed the Ncorr™ free software usefulness to predict the deformation stage for the ECASE process. These results are in good agreement with other investigations where higher shear strains were obtained in the edges of the material like the IF steel processed by differential speed rolling [5]. It was also found that not only the shear strains were higher in the edge vicinities but also the tensile strains in the rolling direction were found to be even higher that the shearing ones.

On the other hand, the Knoop hardness measurements through the sheet thickness corroborated well the Ncorr™ results. The hardness evolution in Fig. 2 allowed seeing some differences between the hardness close to the edges and the core. Besides, it was

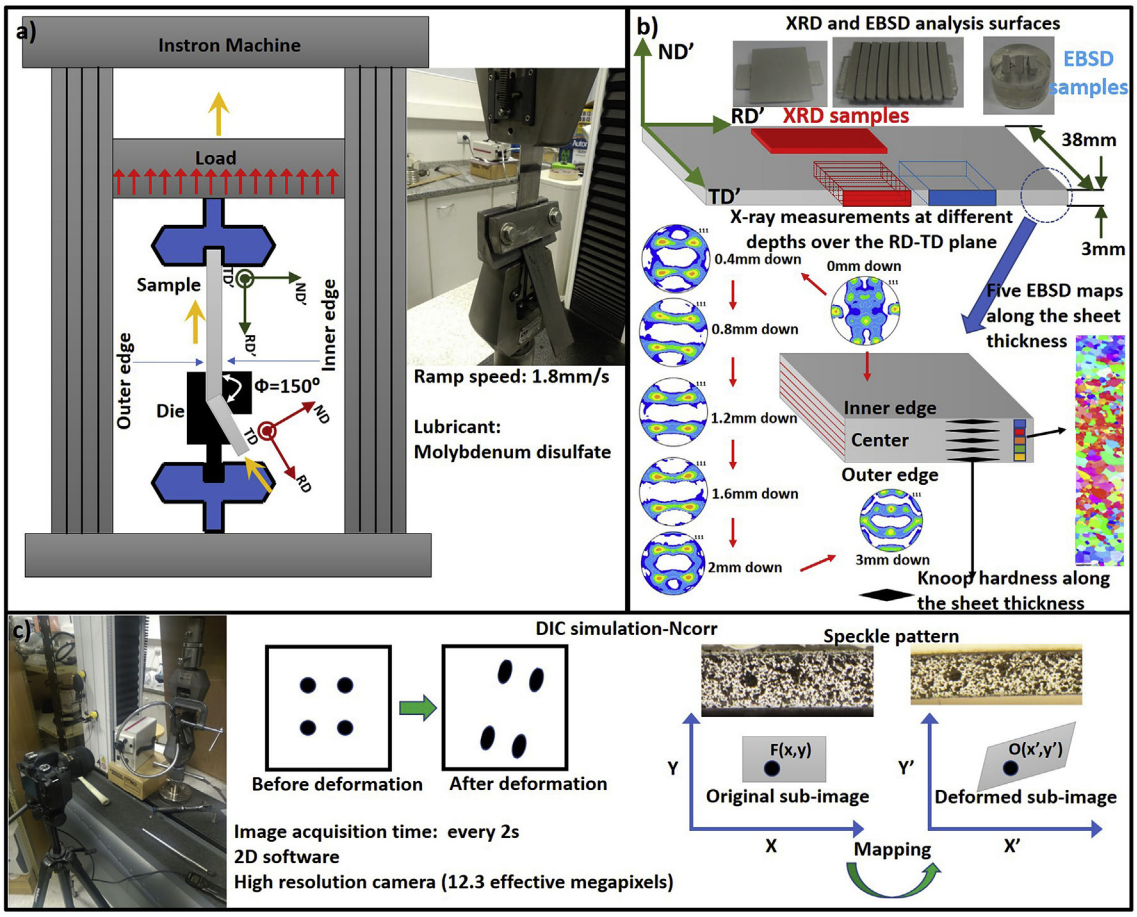

Fig. 1. Experimental procedure a) ECASE process, b) EBSD and X-ray characterization and c) Digital image correlation description.

also seen an overall hardness increase with the aging treatment and after one ECASE pass. After the first ECASE pass, the biggest hardness increments were registered in the regions close to the edges (more intense shearing zones) than in the sheet core (center) where the hardness values are quite similar to the values for the material before deformation. A similar behavior was observed in the study of Fandiño et al. [21] with a magnesium alloy processed by ECASE. The lower overall hardness increase observed in this study in comparison with other studies, such as the one from Khelfa et al. [22] for an Al-Mg-Si alloy processed by ECAP, can be mainly attributed to the lower amount of deformation introduced with each ECASE pass (~0.3 with this ECASE die against 0.66–1.0 for the most common ECAP dies).

3.2. Microstructure and texture

3.2.1. Texture evolution

For understanding and characterizing much better the microstructure and texture evolution during the ECASE process, complete EBSD scans were performed in the rolling plane at different depths through the complete sheet thickness, together with X-ray runs. Texture characterization was done following the ideal texture components for FCC materials (rolling and simple shear texture components) described in Fig. 3, Table 1 [23] and Table 2 [24]. The EBSD scans and the X-ray results can be seen in Fig. 3 for the ECASE processed material. Texture was analyzed in rolling plane (⊥ ND) and shearing plane (⊥ TD) to see the different contributions from rolling and simple shear texture components.

The {111} pole figures in the rolling plane for both EBSD and X-ray diffraction are observed in Fig. 3. The main texture changes can be seen in the pole figures belonging to the inner and outer edge surfaces in the case of X-ray and to S1 and S5 EBSD areas. As it was mentioned before, those zones were the most affected by the shear and rolling strain. On the other hand, in the center of the sheet or in the zones far from the edges (0.8, 1.2, 1.6, 2 mm and S2, S3, S4 for the X-ray and EBSD measurements respectively) a rolling texture was the most dominating.

In Fig. 4, the different texture component contributions from the simple shear and rolling conditions were calculated and compared, analyzing the shearing and rolling planes respectively. Examining the texture components over the rolling plane calculated by X-ray and EBSD it can be seen the strong presence of the Cube component. However, this component was only present in the center of the sheet since it was absent in the areas closer to the edges. The texture intensities showed in Fig. 3 for the pole figures indicate that the highest value was obtained for the texture measured in the sheet core. For that reason, the overall texture measured by X-ray diffraction (see Fig. 4) allowed to see that the dominant texture corresponds well with a recrystallized one with a strong Cube component [25,26], which can be attributed to the aging treatment. Continuing with the rolling components in the zones close to the edges, components like S, Brass, Dillamore, E, rotated Copper and rotated Cube are observed, which are associated with the presence of a rolling texture [27]. A similar behavior was reported by Naseri et al. [28] for a bimodal AA2024 processed by ARB. It is worth mentioning that the strongest component in zones close to the

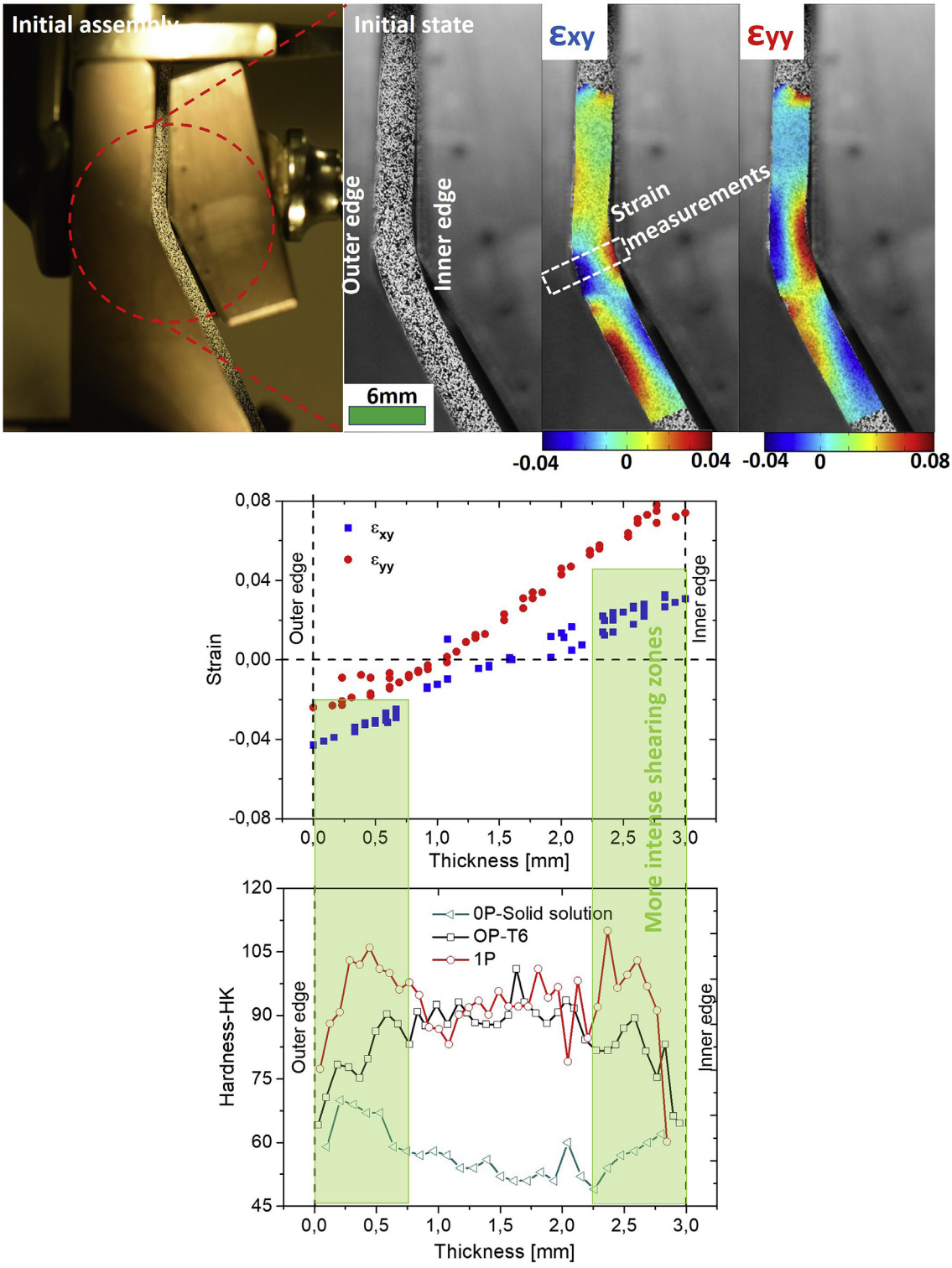

Fig. 2. Strain calculation, its distribution by Ncorr™ software, and hardness evolution along the sheet thickness.

edges was the S component, which was more important in the inner edge zone (inner edge surface or S1 according with the X-ray and EBSD calculations).

In Fig. 4 we can also observe the presence of typical shear texture components like rotated Cube, rotated Copper and E [25,29] in the zones closer to the inner edge but not in the zones of the outer edge. Conversely, the Dillamore component was found to be stronger in the outer edge region than in the inner edge region. The existence of shearing components in the inner edge can be attributed to the higher friction and strains in this zone as was also showed in process like rolling and asymmetrical rolling [30,31]. In this context, it can be observed the existence of texture components related with rolling and shearing in different zones of the sheet (edges and center). The fact that more rolling texture

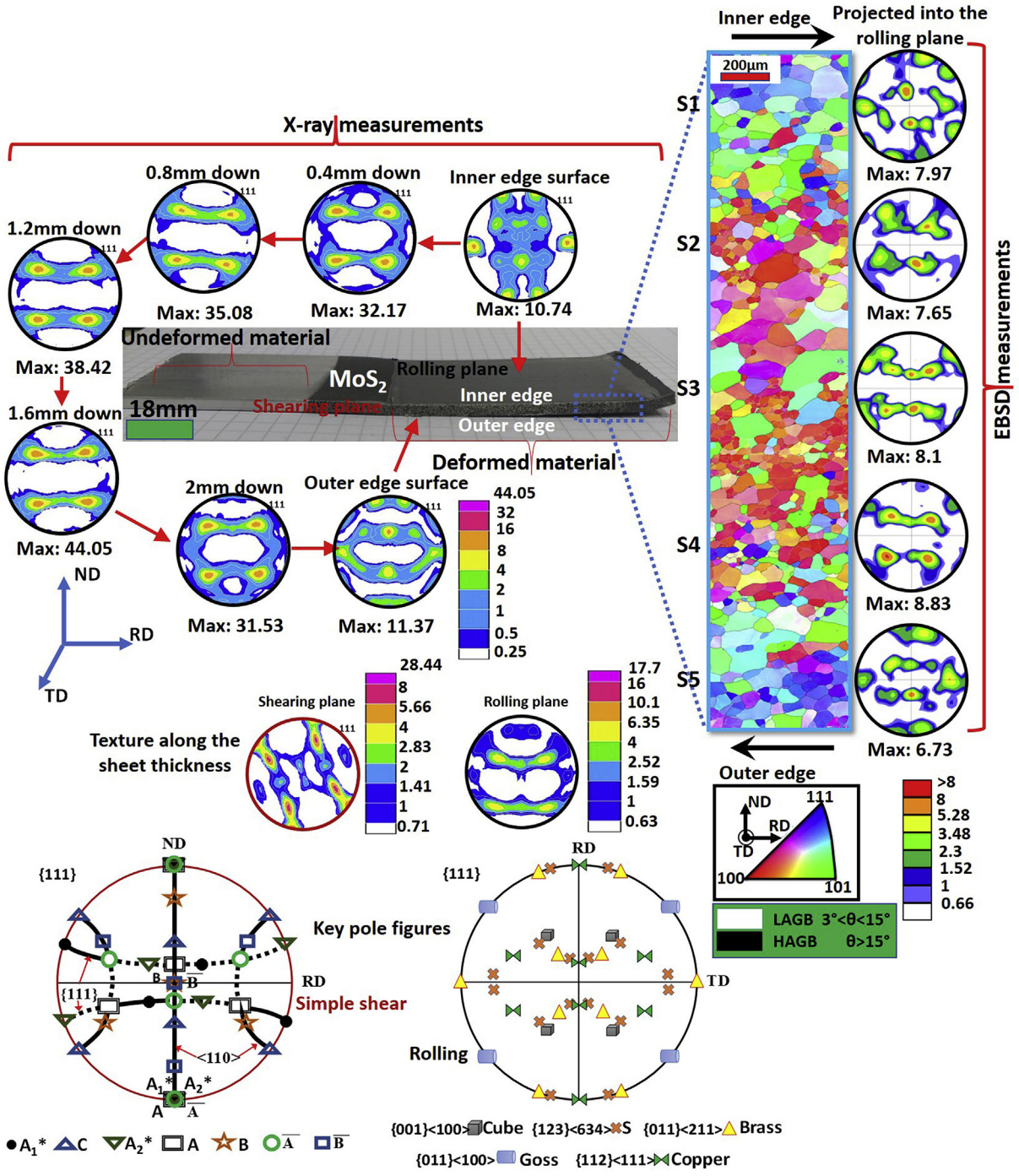

Fig. 3. Texture characterization by EBSD and X-ray diffraction.

components appear in the inner edge that in the outer one can be associated with the higher values of strain following the rolling direction obtained by Ncorr™ in the inner surface.

For knowing much better the ECASE effect over the material texture the simple shear components were also analyzed. In Fig. 4 the volume fraction of the simple shear components for FCC materials obtained by means of X-ray and EBSD are indicated. As a first observation, the intensity of these components is lower than the components calculated in the rolling plane. However, the existence of these components was mainly found in the zones close to the edges where the shear strain due to the ECASE die was also higher. The X-ray measurements showed high volume fractions of the A_1^*, A_2^*, A and $\overline{A}$ components in the inner edge zone while, the B and $\overline{B}$ components presented the most important volume fraction in the outer edge zone. On the other hand, the EBSD measurements indicated the presence of the C component for both inner and outer edge regions.

According with Li et al. [24], the most important ideal orientations in simple shear are found to be distributed along two fibers, one with a crystallographic slip direction parallel to the shear direction and other with a crystallographic slip plane parallel to the shear plane [32]. For fcc materials, they are the {*h k l*} <1 1 0> fiber

Table 1
Ideal texture components for FCC materials.

Texture component	Miller indices	Euler angles		
	{hkl}<uvw>	φ_1	φ	φ_2
Cube	{001}<100>	0	0	0
Rotated cube[a]	{001}<110>	45	0	0
Goss	{011}<100>	0	45	0
Rotated goss	{011}<011>	90	45	0
Goss twin	{113}<332>	90	25	45
Brass	{011}<211>	35	45	0
Goss/brass	{011}<115>	16	45	0
A	{011}<111>	55	45	0
Y[a]	{111}<112>	90	55	45
E[a]	{111}<011>	60	55	45
Copper	{112}<111>	90	35	45
Rotated copper[a]	{112}<011>	0	35	45
Copper twin	{554}<115>	90	74	45
Dillamor[a]	{4411}<11118>	90	27	45
S	{123}<634>	59	37	63
S/brass	{414}<234>	49	40	75

[a] Shearing texture components.

Table 2
Simple shear texture components.

Texture component	Miller indices	Euler angles		
	{hkl}<uvw>	ϕ_1	φ	ϕ_2
A_1^*	{111}<112>	35.26/215.26	45	0
		125.26	90	45
A_2^*	{111}<112>	144.74	45	0
		54.74	90	45
A	{111}<110>	0	35.26	45
$\overline{A}$	{111}<110>	180	35.26	45
B	{112}<110>	0	54.74	45
$\overline{B}$	{112}<110>	60	54.74	45
C	{001}<110>	90	45	0

(or <1 1 0> fiber) and the {1 1 1} <*u* v w> fiber (or {1 1 1} fiber). In this way, the X-ray measurements indicate that in the inner edge region there is a presence of the {1 1 1} fiber (A_1^*, A_2^*, A and $\overline{A}$ components, see key pole figure in Fig. 3) with the A and $\overline{A}$ components as the most representative. Besides, the EBSD measurements allowed to see the presence of the <1 1 0> fiber (A, $\overline{A}$, B, $\overline{B}$ and C) in the outer edge region as well as in the inner one, being the $\overline{B}$ and C components the most representative in each region, respectively.

The poor development of the simple shear texture components in this study, in comparison with the rolling components, can be attributed to the higher inner channel angle used in the ECASE die, what causes that lower shear strains can be introduced in the material. On the other hand, the overall texture highlights a shift of ~15° (see pole figure along the sheet thickness in Fig. 3) along the TD axe. This texture change can be attributed to the shearing effect of the process as in other SPD techniques based on the shear strain such as ECAP [33,34]. However, the local measurements did not show a texture twist of that magnitude following the simple shear texture components.

The correct interpretation of the measured textures requires the dynamic overlap of the correct velocity gradients, according to the already known phenomena of extra spin contribution to texture development. The net effects are the rotation of some components, smearing out of some others and general decrease of the texture strength because of the non-stationary material flux during shearing [35,36].

3.2.2. Microstructure characterization

For the material characterization after deformation by the ECASE process at room temperature, different microstructural characteristics such as the grain size, High Angle Grain Boundaries (HAGB) fractions and Geometrically Necessary Dislocations (GNDs) calculations were made.

3.2.2.1. Grain sizes. With the first ECASE pass the measured grain sizes in the five EBSD areas (S1, S2, S3, S4 and S5) did not show big differences along the sheet thickness with values of 32.3, 31.6, 28.8, 30.3 and 36 μm from S1 to S5. Regarding the HAGB fractions along the sheet thickness, some differences between the edges and the center zone were observed. The lower values of HAGB were obtained in the zones close to the sheet edges (S1 and S5) with values of 25 and 32% respectively. While, the values in the center zone (S2, S3 and S4) were 35, 34, and 45%. Those microstructures changes can be associated with the occurrence of Continuous Dynamic Recrystallization (CDRX) due to the introduction of new grain boundaries, mainly Low Angle Grain Boundaries (LAGB).

As stated by Tóth et al. [37], the process of CDRX develops because of the continued evolution from LAGBs into HAGBs during plastic deformation, where Geometrically Necessary Dislocations (GNDs) are the responsible for creating new grain boundaries. In other words, the evolution in the fraction of HAGB with the deformation is a consequence of the continuous transformation of LAGB since initial stages of processing, thus evolving to geometrically necessary boundaries which are formed and then subdivide the coarse grains into cell blocks [38]. For that reason, after the first ECASE pass, a higher fraction of LAGB was identified in the edges zones. This HAGB distribution in the sheet thickness is coherent with the fact that not only the strain distribution but also the texture evolution indicated a heterogeneous behavior between the zones closer to the edges and the sheet core.

3.2.2.2. Geometrically necessary dislocations (GND). The density of GNDs can be calculated from EBSD data [39,40]. Fig. 5 shows the GND density maps over the full sheet thickness for both, undeformed and one ECASE pass samples. The initial condition does not exhibit any grouping of GNDs, the GNDs over the scanned area looks quite homogeneous with average values of 3.1, 2.7, 2.8, 2.7 and $4 \cdot 10^{12}$ m^{-2} in the different EBSD areas (S1, S2, S3, S4 and S5). This behavior is also corroborated by the GND distributions, which show quite coincident peaks.

After one pass some GNDs grouping is observed close to the edges (S1 or inner edge and S5 or outer edge), where the average values were $1.1 \cdot 10^{13} m^{-2}$ and $9.6 \cdot 10^{12} m^{-2}$ respectively with a maximum value of $4 \cdot 10^{13} m^{-2}$ in both zones. Meanwhile, the averages around the center zones (S2, S3 and S4) indicate values of 6.8, 6.2 and $6.8 \cdot 10^{12} m^{-2}$ with a maximum value in the three zones of $2 \cdot 10^{13} m^{-2}$. The GNDs increase after the first ECASE pass, but more in the edge zones, what can be corroborated in Fig. 5 by the peak shift towards higher values, especially in the zones S1 and S5.

The GNDs increased with deformation, although the maximum values are smaller than the values obtained with other SPD techniques like ECAP [37,41] and HPT [42], where the average and maximum values are around the order of $10^{14} m^{-2}$ and $10^{15} m^{-2}$ respectively. Those differences can be related with the higher amount of deformation introduced and the hydrostatic pressures involved in these processes, especially in HPT. As stablished by some researchers [37,43], the higher hydrostatic pressures favored the dislocation multiplication instead of their annihilation.

Once again, based in the GND analysis we can observe that, as in the strain distribution and texture analysis, the differences between the edges and the sheet core visible. Such high-density values of GNDs in deformed materials indicate an excellent potentiality for the grain size reduction, taking into consideration that the GNDs are responsible for grain subdivision [42]. Therefore,

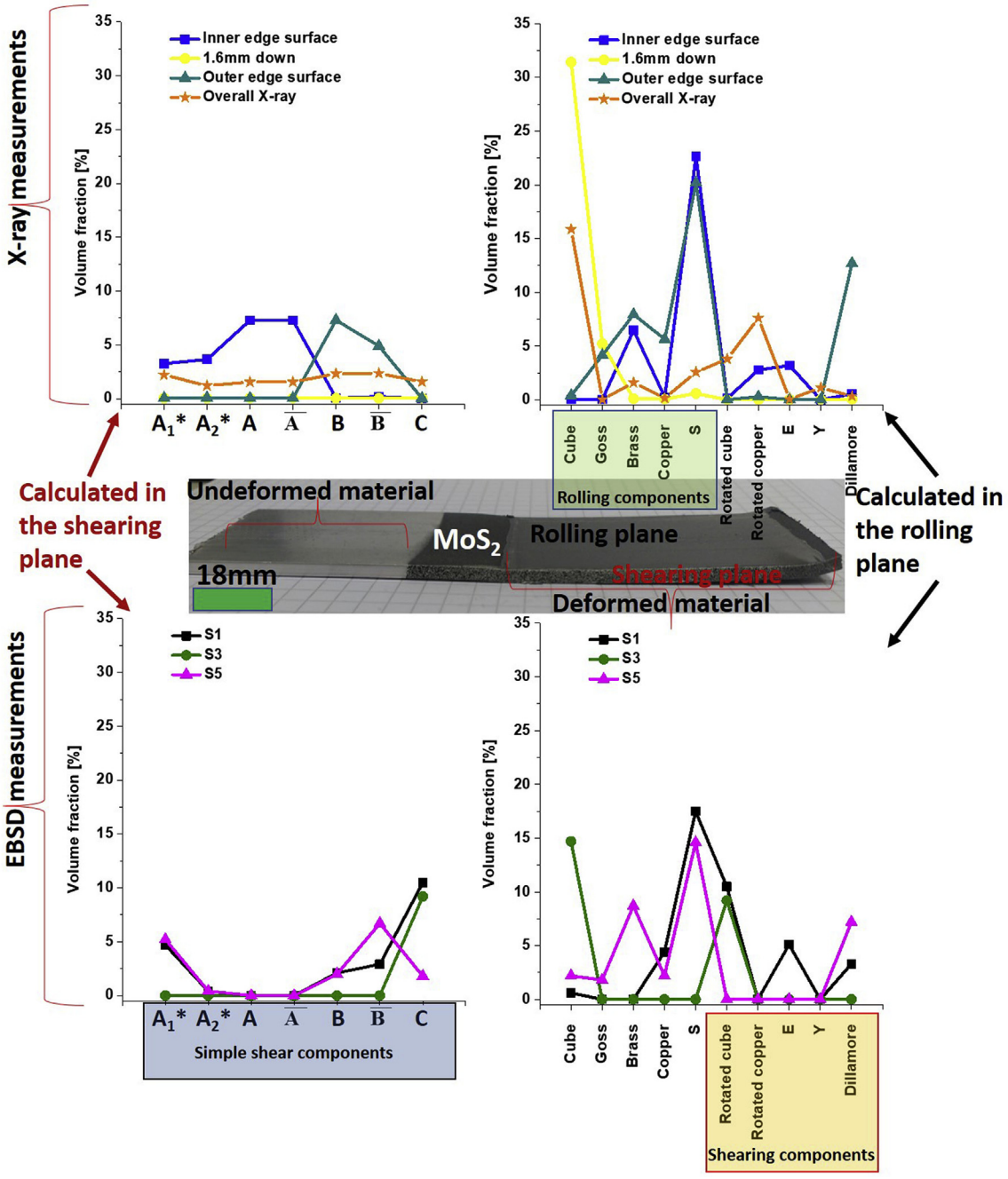

Fig. 4. Texture components evolution for the material with one ECASE pass.

these high-density values of GNDs close to the edges after one ECASE pass show that this technique can be a good alternative to produce a heterogeneous microstructure where both strength and ductility can coexist.

4. Conclusions

A 6063-T6 Al alloy was processed by ECASE at room temperature in one pass. The strain distribution along the sheet thickness was obtained by digital image correlation with Ncorr™ free software. This analysis showed higher strains in the zones closer to the sheet edges and the lowest in the sheet core. In this way, a material with heterogeneous deformation was produced by ECASE.

As a first approximation to corroborate the heterogeneity in the material, the Knoop hardness test indicated differences between the measurements in the zones closer to the edges and the sheet core, with the highest increments in the neighborhoods of the edges.

Texture analysis by X-ray and EBSD allowed to corroborate the existence of texture changes between the edges and the sheet core. With the X-ray and EBSD measurements, it was found that the zones far from the edges presented a recrystallization texture with a Cube component as the most representative. However, texture measurements in the neighborhoods of the edges indicated the presence of a texture mix of rolling (rotated Cube, rotated Copper, E and Dillamore) and simple shear texture components (mainly

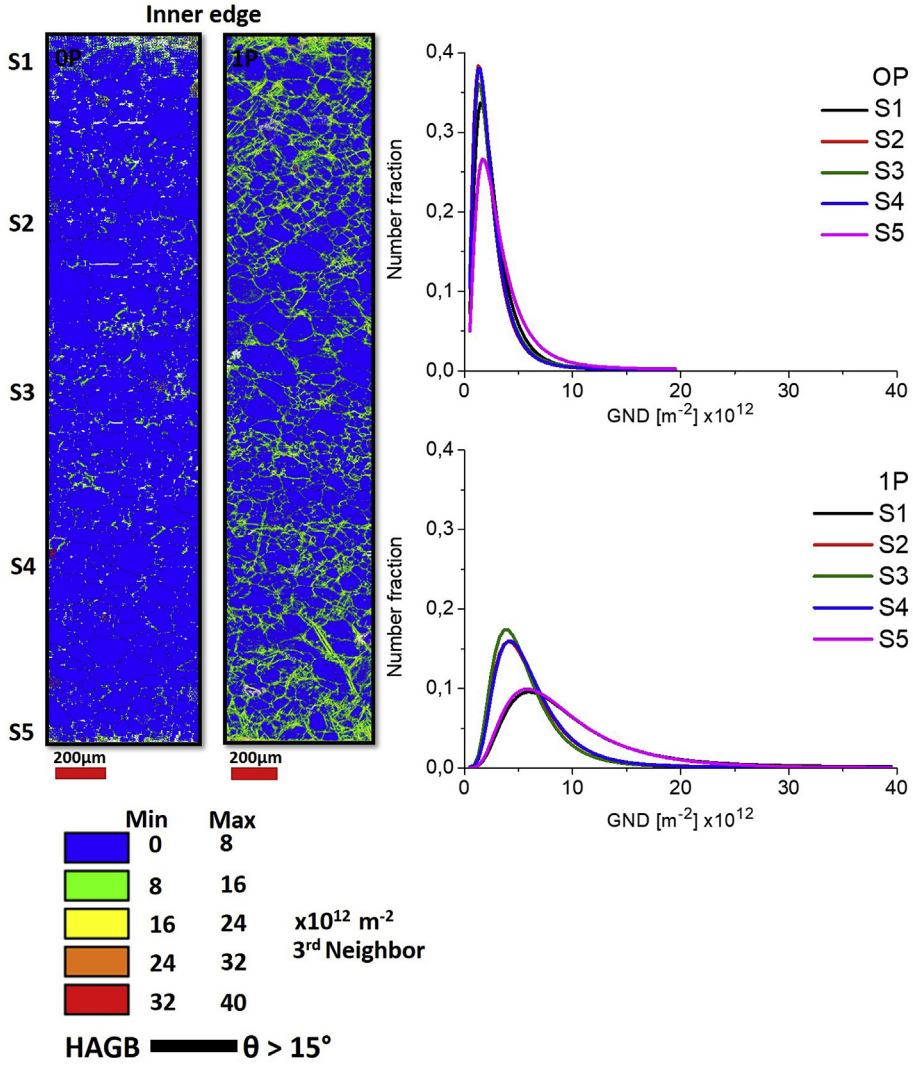

Fig. 5. GNDs evolution for the initial and one ECASE pass along the sheet thickness.

components of {1 1 1} fiber in the inner edge and components of the <1 1 0> fiber in the outer one) due to the high strains located in these zones.

The microstructure in the five zones presented a quite similar grain size with the increment in the fraction of LAGB in the edges zones because of the CDRX phenomenon was taken place. The GNDs evolution confirmed the possibility to get a heterogeneous microstructure (a mix of big and small grains) with the ECASE process due to higher dislocation densities in regions closer to the sheet edges. The technique is very promising in this aspect.

Acknowledgements

JAMB thanks the Latin-American Postdoctoral scholarship (Grant number CONICET D 4263) received by the Argentine Ministry of Science, Technology and Productive Innovation and the National Council of Scientific and Technical Research (CONICET).

References

[1] J. Han, K. Oh, J. Lee, Effect of accumulative strain on texture evolution in 1050 Al alloys processed by continuous confined strip shearing, Mater. Sci. Eng. A 387 (2004) 240–243.
[2] F.Z. Hassani, M. Ketabchi, Nano grained AZ31 alloy achieved by equal channel angular rolling process, Mater. Sci. Eng. 528 (2011) 6426–6431.
[3] A. Zisman, V. Rybin, S. Van Boxel, M. Seefeldt, B. Verlinden, Equal channel angular drawing of aluminium sheet, Mater. Sci. Eng. 427 (2006) 123–129.
[4] E. Bruder, Mechanical properties of ARMCO iron after large and severe plastic deformation—application potential for precursors to ultrafine grained microstructures, Metals 8 (2018) 191.
[5] J.H. Park, K. Hamad, I.P. Widiantara, Y.G. Ko, Strain and crystallographic texture evaluation of interstitial free steel cold deformed by differential speed rolling, Mater. Lett. 147 (2015) 38–41.
[6] E. Ma, T. Zhu, Towards strength–ductility synergy through the design of heterogeneous nanostructures in metals, Mater. Today 20 (2017) 323–331.
[7] M.F. Ashby, The deformation of plastically non-homogeneous materials, Philos. Mag. 21 (1970) 399–424.
[8] T. Sheppard, Extrusion of Aluminium Alloys, Springer Science & Business Media., 2013.
[9] Z. Zeng, X. Li, D. Xu, L. Lu, H. Gao, T. Zhu, Gradient plasticity in gradient nano-grained metals, Extrem. Mech. Lett. 8 (2016) 213–219.
[10] R.Z. Valiev, T.G. Langdon, Principles of equal-channel angular pressing as a processing tool for grain refinement, Prog. Mater. Sci. 51 (2006) 881–981.
[11] A.P. Zhilyaev, T.G. Langdon, Using high-pressure torsion for metal processing: fundamentals and applications, Prog. Mater. Sci. 53 (2008) 893–979.
[12] Y.M. Saito, H. Utsunomiya, N. Tsuji, T. Sakai, Novel ultra-high straining process for bulk materials—development of the accumulative roll-bonding (ARB) process, Acta Mater. 47 (1999) 579–583.
[13] S. Suwas, R.K. Ray, Crystallographic Texture of Materials, Springer-Verlag, London, 2014.
[14] H.J. Bunge, Fabric analysis by orientation distribution functions, Tectonophysics 78 (1981) 1–21.
[15] L.G. Schulz, A direct method of determining preferred orientation of a flat reflection sample using a geiger counter x-ray spectrometer, J. Appl. Phys. 20

(1949) 1030.
[16] D. Chateigner, P. Germi, M. Pernet, Texture analysis by the Schulz reflection method: defocalization corrections for thin films, J. Appl. Cryst. 25 (1992) 766–769.
[17] J.S. Kallend, U.F. Kocks, A.D. Rollett, H.R. Wenk, Operational texture analysis, Mater. Sci. Eng. A 132 (1991) 1–11.
[18] F. Bachmann, R. Hielscher, H. Schaeben, Texture analysis with MTEX - free and open source software toolbox, Solid State Phenom. 160 (2010) 63–68.
[19] J. Blaber, B. Adair, A. Antoniou, Ncorr: open-source 2D digital image correlation matlab software, Exp. Mech. 55 (2015) 1105–1122.
[20] A.F. Ab Ghani, M.B. Ali, S. DharMalingam, J. Mahmud, Digital image correlation (DIC) technique in measuring strain using opensource platform Ncorr, J. Adv. Res. Appl. Mech. 26 (2016) 10–21.
[21] E.M. Fandiño, R.E. Bolmaro, P. Risso, V. Tartalini, P.F. Morales, M. Ávalos, Microstructure, and surface mechanical properties of AZ31 magnesium alloys processed by ECASD, Adv. Eng. Mater. (2017), 1700228.
[22] T. Khelfa, M.A. Rekik, J.A. Muñoz-Bolaños, J.M. Cabrera-Marrero, M. Khitouni, Microstructure and strengthening mechanisms in an Al-Mg-Si alloy processed by equal channel angular pressing (ECAP), Int. J. Adv. Manuf. Technol. (2017) 1–13.
[23] R. Jamaati, M.R. Toroghinejad, Effect of stacking fault energy on deformation texture development of nanostructured materials produced by the ARB process, Mater. Sci. Eng. 598 (2014) 263–276.
[24] S. Li, I.J. Beyerlein, M.A.M. Bourke, Texture formation during equal channel angular extrusion of fcc and bcc materials: comparison with simple shear, Mater. Sci. Eng. 394 (2005) 66–77.
[25] F. Humphreys, M. Hatherly, Recrystallization and Related Annealing Phenomena, Pergamon, Oxford,United Kingdom, 1996.
[26] S. De La Chapelle, P. Duval, Recrystallization in a hot deformed Al-Mg-Si alloy: T he effect of fine precipitates, Textures Microstruct. 35 (2002) 55–70.
[27] O. Engler, V. Randle, Introduction ToTexture Analysis – Macrotexture, Microtexture, and Orientation Mapping, second ed., United States of America: Taylor & Francis Group, 2010.
[28] M. Naseri, M. Reihanian, E. Borhani, A new strategy to simultaneous increase in the strength and ductility of AA2024Nalloy via accumulative roll bonding (ARB), Mater. Sci. Eng. 656 (2016) 12–20.
[29] H.W. Kim, S.B. Kang, N. Tsuji, Y.M. Amino, Deformation textures of AA8011 aluminum alloy sheets severely deformed by accumulative roll bonding, Metall. Mater. Trans. 36 (2005) 3151–3163.
[30] H. Jin, D.J. Lloyd, The different effects of asymmetric rolling and surface friction on formation of shear texture in aluminium alloy AA5754, Mater. Sci. Technol. 26 (2009).
[31] H.K. Kim, H.W. Kim, J.H. Cho, J.C. Lee, High-formability Al alloy sheet produced by asymmetric rolling of strip-cast sheet, Mater. Sci. Eng. 574 (2013) 31–36.
[32] G.R. Canova, U.F. Kocks, J.J. Jonas, Theory of torsion texture development, Acta Metall. 32 (1984) 211–226.
[33] I.J. Beyerlein, L.S. Tóth, Texture evolution in equal-channel angular extrusion, Prog. Mater. Sci. 54 (2009) 427–510.
[34] L.S. Tóth, Texture evolution in severe plastic deformation by Equal Channel angular extrusion, Adv. Eng. Mater. 5 (2003) 308–316.
[35] R.E. Bolmaro, U.F. Kocks, A comparison of the texture development in pure and simple shear and during path changes, Scripta Metall. Mater. 27 (1992) 1717–1722.
[36] M.C.V. Vega, R.E. Bolmaro, M. Ferrante, V.L. Sordi, A.M. Kliauga, The influence of deformation path on strain characteristics of AA1050 aluminium processed by equal-channel angular pressing followed by rolling, Mater. Sci. Eng. 646 (2015) 154–162.
[37] L. Tóth, C. Gu, Ultrafine-grain metals by severe plastic deformation, Mater. Char. 92 (2014) 1–14.
[38] Y. Tomita, K. Okabayashi, Tensile stress-strain analysis of cold worked metals and steels and dual-phase steels, Metall. Trans. A 16 (1985) 865.
[39] W. Pantleon, Resolving the geometrically necessary dislocation content by conventional electron backscattering diffraction, Scripta Mater. 58 (2008) 994–997.
[40] J.F. Nye, Some geometrical relations in dislocated crystals, Acta Metall. 1 (1953) 153–162.
[41] J.A. Muñoz, O.F. Higuera, J.M. Cabrera, High cycle fatigue of ARMCO iron severely deformed by ECAP, Mater. Sci. Eng. 681 (2017) 85–96.
[42] A. Pougis, L.S. Toth, J.J. Fundenberger, A. Borbely, Extension of the Derby relation to metals severely deformed to their steady-state ultrafine-grain size, Scripta Mater. 72 (2014) 59–62.
[43] J.L. Sturges, B. Parsons, B.N. Cole, Mechanical properties at high rates of strain, Inst. Phys. Conf. 47 (1980) 35–48.